GEOPHYSICS, VOL. 86, NO. 1 (JANUARY-FEBRUARY 2021); P. E59–E75, 10 FIGS., 2 TABLES.
10.1190/GEO2019-0552.1

Investigation of cable effects in spectral induced polarization imaging at the field scale using multicore and coaxial cables

Adrian Flores Orozco[1], Lukas Aigner[1], and Jakob Gallistl[1]

ABSTRACT

The spectral induced polarization (SIP) method has emerged as a well-suited laboratory technique to characterize hydrogeologic and biogeochemical parameters in soil samples. However, field applications of the SIP imaging method are still rare, which can be attributed to the particular care required to minimize the contamination of the data by electromagnetic coupling. To date, field procedures rely on the use of two different cables separating the current and potential dipoles to improve the quality of the SIP readings, although this increases the efforts in the field and might reduce the depth of investigation or the spatial resolution of the data. To overcome these limitations, we have investigated the use of a single coaxial cable, as an alternative to improve data quality and simplify field procedures. We evaluate SIP imaging data collected with the same measuring device using a coaxial cable and a combination of multicore cables of different lengths and manufacturers. Data sets collected with a single coaxial cable reveal a significantly lower number of outliers and a high spatial consistency between the phase-lag readings, even for measurements collected with a coaxial cable five times longer than the length of the profile. Furthermore, the data collected with coaxial cables reveal an improved quality for deeper measurements (with a lower signal-to-noise ratio) in comparison to data sets collected with separate cables. Our results demonstrate that the use of coaxial cables might permit the collection of SIP readings with high quality and similar field procedures to those used in resistivity surveys.

INTRODUCTION

Induced polarization (IP) is an extension of the DC-resistivity method, which provides information about the conductive and capacitive properties of the subsurface. The measurements can be collected at different frequencies, in the so-called spectral IP (SIP) method, to gain information about the frequency dependence of the electrical properties, commonly in the frequency range between 0.06 and 1000 Hz (e.g., Kemna et al., 2012; Flores Orozco et al., 2018a). Traditionally, SIP measurements are performed in the frequency-domain (FD), with imaging measurements deploying tens to hundreds of electrodes to perform thousands of readings based on four-electrode arrays (for further details on the method, see Binley and Kemna, 2005; Kemna et al., 2012). Taking into account the strong IP effect (hereafter referred to as polarization) of metallic minerals under the application of an external electrical field, SIP is a method commonly used for the prospection of mineral ores, among other mining applications (Pelton et al., 1978; Seigel et al., 2007). Developments in the accuracy of the measuring instruments (e.g., Zimmermann et al., 2008) and in the modeling algorithms (e.g., Binley and Kemna, 2005; Kemna et al., 2012; Günther and Martin, 2016) have permitted extension of the application of the SIP method to investigate processes and materials associated with much weaker polarization responses. To date, the SIP method has been applied in a variety of engineering, hydrogeologic, and environmental investigations (Kemna et al., 2012; Revil et al., 2012a; Binley et al., 2015; Flores Orozco et al., 2018a; Gallistl et al., 2018). In particular, within the past two decades, extensive laboratory studies have demonstrated a strong link between the SIP parameters and soil properties controlling water flow, therefore permitting the quantification of hydraulic conductivity (e.g., Börner et al., 1996; Revil and Florsch, 2010; Weller et al., 2010; Binley et al., 2016). In addition, laboratory experiments have demonstrated the sensitivity of the SIP measurements to parameters of relevance accompanying different biological and geochemical processes in the emerging

Manuscript received by the Editor 30 August 2019; revised manuscript received 30 September 2020; published ahead of production 14 October 2020; published online 20 January 2021.
[1]TU-Wien, Department of Geodesy and Geoinformation, Geophysics Research Division, Vienna 1040, Austria. E-mail: adrian.flores-orozco@geo.tuwien.ac.at (corresponding author); lukas.aigner@geo.tuwien.ac.at; jakob.gallistl@geo.tuwien.ac.at.

DOI:10.1190/geo2019-0552.1

discipline of biogeophysics (Atekwana and Slater, 2009 for further references). Among these processes are the stimulation of microbial activity (e.g., Ntarlagiannis et al., 2005; Williams et al., 2005; Slater et al., 2007), the accumulation of biofilms (Aal et al., 2006; Revil et al., 2012b), and more recently, the geometry and growth of root systems (e.g., Corona-Lopez et al., 2019; Weigand and Kemna, 2019).

However, to date, SIP field applications are still rare. The necessity to collect data at different frequencies leads to significantly longer acquisition time for FD SIP imaging surveys than for standard electrical resistivity tomography (ERT), especially for data collected at low frequencies (<1 Hz). Long acquisition times may hinder the collection of broadband SIP data in surveys performed under time constraints. Hence, some studies have reported field IP data collected only at a single frequency — or a few frequencies, for instance, for the monitoring of groundwater remediation by means of nanoparticle injections (Flores Orozco et al., 2015, 2019a), or for the investigation of bioremediation techniques (e.g., Williams et al., 2009; Flores Orozco et al., 2011). To date, broadband FD SIP imaging at the field scale has been reported for the estimation of hydraulic conductivity (Hördt et al., 2007), the monitoring of microbial activity during the immobilization of radionuclides (Flores Orozco et al., 2013), the delineation of hydrocarbon-impacted sites (Flores Orozco et al., 2012a), the investigation of landslides (Flores Orozco et al., 2018a; Gallistl et al., 2018), and — at smaller spatial scales — to detect fungi infection in trees (Martin and Günther, 2013). Recent studies have demonstrated that parameters describing the frequency dependence of the IP effect can also be retrieved from time-domain IP (TDIP) data, if the measurements record the full waveform and the inversion is performed with modern algorithms, opening the technique to new possibilities (e.g., Fiandaca et al., 2018; Olsson et al., 2019). Still, long pulse lengths (i.e., acquisition time) are required to gain information at low frequencies associated to slow polarization processes.

SIP surveys at high frequencies (i.e., above 1 Hz) are related to short acquisition times; yet they are subject to contamination of the data due to parasitic electromagnetic (EM) fields, commonly referred to as EM coupling (e.g., Pelton et al., 1978). EM coupling increases proportionally with the acquisition frequencies, and it is expected to contaminate measurements collected above 10 Hz (Wait and Gruszka, 1986; Binley et al., 2005; Kemna et al., 2012). Nonetheless, some studies have already observed that EM coupling dominates the SIP response at frequencies at approximately 5 Hz (e.g., Kemna et al., 2000; Gasperikova and Morrison, 2001; Williams et al., 2009; Flores Orozco et al., 2011).

EM coupling is caused by either inductive or capacitive sources (e.g., Zimmermann et al., 2008, 2019). Capacitive coupling (i.e., involving displacement currents) results from differences in the contact impedances between the electrodes and the subsurface or between the conductive shield of the cables and the surface, resulting in leakage currents (e.g., Zimmermann et al., 2008, 2019; Zhao et al., 2013, 2014). Capacitive EM coupling can also arise due to voltage differences between the cables used for voltage measurements and those used for current injection. The capacitive EM coupling (EM_{cc}) between parallel cables (of an infinite length) and an electrical field can be calculated (Charnock, 2005) as

$$EM_{cc} \cong \frac{\pi \varepsilon_0}{\ln(D/a)}, \tag{1}$$

where D is the distance between the cables, a is the cable radius, and ε_0 is the electrical permittivity of free space.

Inductive coupling is related to temporal variations in the current flow (i.e., that produced by a magnetic field) along the wires connecting the electrodes and the measuring device, which result in the induction of parasitic fields in conductive materials (e.g., conductive soils, metallic wires in multicore cables). The inductive coupling is known to be proportional to the conductivity of the subsurface, the acquisition frequency, and the square of the cable length (e.g., Hallof, 1974; Pelton et al., 1978). Hence, many approaches have been suggested for the decoupling of SIP readings by removing the influence in the data of inductive fields associated with layered media and the cable geometry (e.g., Hallof, 1974; Coggon, 1984; Wait and Gruszka, 1986; Routh and Oldenburg, 2001; Zhao et al., 2013). Yet, inductive coupling can also take place within the cable bundle used in SIP field surveys. Assuming parallel cables with an infinite length and without considering coupling with the subsurface, the inductive coupling (EM_{ic}) can be calculated by

$$EM_{ic} \cong 0.1 \cdot \ln\left(1 + \left(\frac{2h}{D}\right)^2\right), \tag{2}$$

where h refers to the height of the conductors relative to the earth plane. EM coupling between the cables represents an inherent problem in SIP imaging applications, which to date still relies on the deployment of tens to hundreds of cable cores (i.e., one for each electrode), with the cable length increasing for deeper investigations.

To facilitate data collection at the field scale, the use of multicore cables is a common practice because these are easier to handle than separate wires and are low maintenance, permitting the collection of data in practically all environments from frozen rocks to landslides (e.g., Doetsch et al., 2015; Gallistl et al., 2018). However, the isolation between the independent wires might not provide enough separation to avoid coupling within the multicore cable. Some alternatives have been proposed, for instance, to digitize the response directly at the electrode using so-called remote units minimizing crosstalking between the transmitter and the receiver, or between the cables (Radic, 2016). However, commercially available instruments lack the robustness and flexibility of multicore cables, involve complicated field procedures, and limit the application of the method in rough terrains and for the mapping of extensive areas. The use of separate cables for current injection and potential readings (Dahlin et al., 2002) reduces the contamination of the data due to coupling within the cables by increasing their separation. However, such practice either reduces the depth of investigation or the resolution of the measurements. In the case that each electrode position requires two cables to separate current and voltage dipoles, the length of the profile is reduced by half and, thus, so is the nominal depth of investigation. Alternatively, it is possible to double the separation between electrodes in the multicore cables and alternate each cable and position with one potential and one current electrode to keep the length of the profile and still permit the use of two separate cables. However, this procedure increases the dipole length and consequently reduces the resolution of the imaging data set. Moreover, the separation between the separate cables needs to be large enough to minimize crosstalk (Telford et al., 1990). Alternatively, the use of shielded cables has been suggested to minimize capacitive crosstalking and inductive coupling between wires (Telford et al., 1990), which to date are deployed in some laboratory

DOI:10.1190/geo2019-0552.1

instruments. However, besides rare examples (e.g., Flores Orozco et al., 2013), such a practice has not been widely implemented in field investigations. Recent investigations (e.g., Zhao et al., 2013, 2014; Huisman et al., 2016; Zimmermann et al., 2019) have proposed different techniques to model the EM response and correct SIP data at high frequencies; however, such methods require detailed knowledge on the geometric wire layout, which may hinder its application for large-scale surveys. Moreover, correction of the data does not substitute for proper field procedures.

Although the quality of the SIP readings over a broad frequency range is critical to extend the observations from the laboratory to the field scale, to date, few studies have addressed in detail the field procedures to enhance data quality in field FD SIP readings (see Dahlin et al., 2002; Flores Orozco et al., 2013; Huisman et al., 2016; Zimmermann et al., 2019). In this regard, there is a considerable gap between laboratory and field-scale studies addressing the methodologies for the collection of SIP data with high quality. In particular, the use of coaxial cables for the collection of field-scale SIP imaging data sets has not been evaluated in detail, even if this is a common practice for laboratory studies (e.g., Zimmermann et al., 2008; Huisman et al., 2016). Hence, in this study, we compare SIP imaging measurements performed with coaxial and standard multicore cables aiming at proposing a simplification of the field procedures for the collection of field SIP imaging with high quality. To better investigate cable effects, we compare measurements collected with a variety of multicore cables (covering different lengths and manufacturers) using a single layout and separate cables for current and potential dipoles.

The general expectation in our experimental setup is that SIP measurements collected with the same measuring device, under the same field conditions, and using the same electrodes, should result in nearly identical imaging data sets, even if the multicore cables are produced by different manufacturers. Likewise, we also assume that the EM coupling between the cables and the ground is the same. Such an expectation should be valid at least for data collected below 10 Hz, in which EM coupling is commonly assumed to be negligible. Consequently, distortions in the data can be only attributed to cable effects (i.e., inductive and capacitive coupling within the cables). Imaging data sets are compared with those collected with coaxial cables to investigate their benefits in field SIP imaging surveys. For completeness, we also investigate possible cable effects by deploying coaxial and different multicore cables (and setups) for the collection of TDIP measurements. We also present an analysis of the normal and reciprocal misfit for readings collected with multicore and coaxial cables to quantitatively compare variations in data error associated to the different cables.

MATERIALS AND METHODS

We compare here the readings collected with three multicore cables purchased from different companies: Iris Instruments, Multi-Phase Technologies (MPT), and Pro-Seismic Services, which are hereafter referred to as MCX, MCY, and MCZ. For our measurements, we considered cables with 32 takeouts (i.e., electrodes) and mainly two different spacings between them: 5 and 1 m, referred to as the long and short cables, respectively. Accordingly, we refer to the different multicore cables as MCX5, MCY5, MCZ5, MCX1, and MCZ1, corresponding to the different manufacturers and the separation between takeouts. To extend the comparison, TDIP measurements were also collected using coaxial and different multicore cables. Table 1 presents a summary of the different cables deployed and the corresponding names.

The coaxial cable used in this study was constructed at the Technical University of Vienna (TU-Wien) using 32 independent wires with lengths between 5 and 155 m, yielding 32 takeouts at 5 m separation between them, hereafter referred to as COAX5. The coaxial cables were twisted together and taped with thermal adhesive tape to form a single bundle and permit easy handling. In this way, the coaxial cable can be rolled into a cable reel and be used in the field in the same way as a multicore cable (see Figure 1). To investigate the effect in the data by deploying coaxial cables with different lengths, two additional coaxial cables were manufactured with separations of 2 and 10 m between takeouts (COAX2 and COAX10), for total lengths of 62 and 310 m, respectively. During the construction of each coaxial bundle, particular care was taken to connect the shield of each coaxial cable to the metallic plug to be connected with a measuring device, which has a ground connection through an external electrode (see Figure 1). Accordingly, the shields of the cables have the same voltage at the connection point to reduce EM coupling. The coaxial cable deployed here is a coaxial RG-174 A/U, with a characteristic impedance of 50 ± 2 Ω, a capacitance of 101 pF/m, a propagation rate of 66%, and attenuation of 40 dB/100 m at 200 MHz. The outside diameter of the conductor is 0.48 mm, the internal diameter of the shield is 1.95 mm, and the entire cable has a diameter of 2.7 mm. The dielectric insulator is polyethylene, with a dielectric constant of 2.4 ± 0.1 and a relative magnetic permeability of 1 ± 0.05. The cable has a copper index of 5.4 kg/km and a weight of 12 kg/km.

For the collection of IP readings, we deployed a data acquisition system (DAS-1) instrument from MPT, which performs the TDIP and FDIP measurements. Consequently, we can investigate the influence of the cable effects on the data quality for both measuring techniques based on the same instrument. Our measurements were collected along two profiles, each with 32 stainless steel electrodes: profile P1, with a separation of 5 m between electrodes and roughly

Table 1. Summary of the geometric characteristics and physical properties of the different multicore (MC) and coaxial (COAX) cables used in this study.

Cable ID	Total length (m)	Takeout spacing (m)	Resistance (Ω)	Capacitance (F)
MCX5	183.8	5	13.8	15.4
MCX1	38.3	1	2.9	3.9
MCY5	159.8	5	8.2	9.7
MCZ10	320	10	67.5	19.7
MCZ5	170	5	36	7.4
MCZ1	40.5	1	9.8	2.2
COAX2	64	2	0.3 Ω/m	0.1 nF/m
COAX5	157	5	0.3 Ω/m	0.1 nF/m
COAX10	152	10	0.3 Ω/m	0.1 nF/m

For the capacitance of the multicore cables, we refer to the measured values between two adjacent wires in the end connector, whereas for coaxial cables, we refer to the values provided by the manufacturer as each cable has different length. Accordingly, the resistance and capacitance values in the coaxial cables are given as a function of their length.

DOI:10.1190/geo2019-0552.1

oriented north to south and profile P2, perpendicular to P1, with a separation of 1 m between electrodes. SIP data were collected in the frequency range between 0.5 and 225 Hz, whereas IP data in the time domain were collected with 0.5 s pulse length. This pulse length was selected because the EM coupling is expected to affect readings at frequencies above 1 Hz, i.e., in the early times. Hence, a pulse length of 0.5 s permits us to use the 35 sampling gates available in the DAS-1 device to capture the voltage decay at early times (i.e., just 20 ms after shutting the current off), which are the most affected by EM cable effects. Measurements were acquired with a dipole-dipole (DD) skip-0 configuration, meaning that the length of the current and potential dipoles is equal to the electrode spacing (as illustrated in Figure 2). Electrodes used for voltage measurements were always located ahead of the current dipole to avoid contamination of the IP readings due to polarization of the electrodes (e.g., Slater et al., 2000; Flores Orozco et al., 2018a). Our configuration contains a total of 435 quadrupoles covering between 1 and 29 levels, with the levels referring to the number of electrodes separating current and potential dipoles (as illustrated in Figure 2). This configuration was selected to record data with a large range in the transfer resistances aiming at capturing a large dynamic range in the S/N in our measurements. In this study, we do not discuss electrode configurations characterized by higher S/N, for instance, with a larger dipole length (DD skip > 0) because they do not provide further insights into the cable effects in the data. Moreover, the comparison of different electrode configurations in SIP imaging has been addressed in previous studies (e.g., Flores Orozco et al., 2018b).

Figure 1. Coaxial cable (COAX2) used in this study, with the picture presenting (a) the twisting and tightening of the cable to make a single bundle, (b) the pins in the end connector referred to in the laboratory measurements, and (c) the attachment of the shields of the independent cables into the end connector to permit their grounding through an external electrode and, thus, leveling the voltages of the individual cable shields at the end connector.

We collected the measurements presented here at the Hydrological Open Air Laboratory (HOAL) located in Lower Austria (Austria). The HOAL site is a small catchment (66 ha), where different investigations are being conducted to understand runoff generation (Blöschl et al., 2016). The SIP data sets presented in this study were acquired in a forest-covered area characterized by heavy soils (clay and silt content above 70%). Due to the high content of fine particles, the electrical properties at the low frequencies (<100 Hz) are expected to be dominated by conduction (i.e., the real component of the surface conductivity) over polarization (i.e., the imaginary component of the surface conductivity) due to the contribution of ionic and surface conduction mechanisms. However, at the selected location, previous measurements have revealed relatively high phase-lag readings ($-\phi > 10$ mrad) attributed to a biogeochemically active zone, which has been validated through analysis in the laboratory of recovered sediments after drilling (see Figure 3). Hence, the study area offers an excellent opportunity to investigate cable effects in SIP imaging measurements. On the one hand, conductive

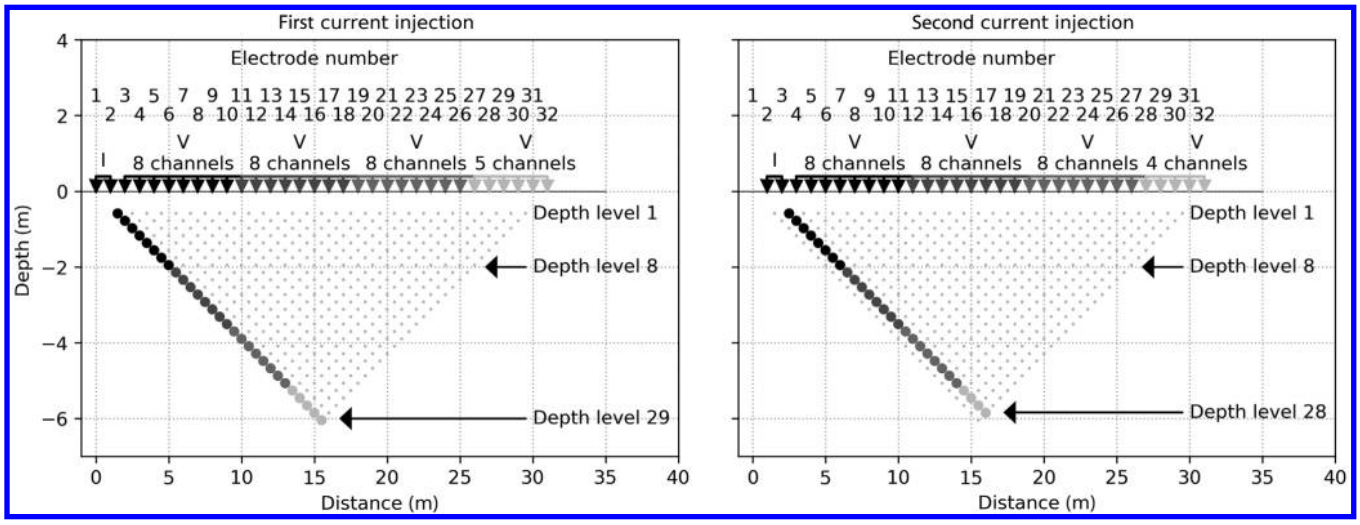

Figure 2. Representation of the dipole-dipole skip-0 configuration used in this study considering 32 electrodes, with all possible voltage measurements (indicated as V) for a given current dipole (indicated as I) and the levels representing the distance (given in terms of the electrode spacing) between the current and potential dipole.

DOI:10.1190/geo2019-0552.1

soils are commonly related to high coupling effects (e.g., Hallof, 1974). On the other hand, changes in subsurface properties lead to a polarizable anomaly, thus enhancing the S/N. A detailed interpretation of the electrical response of the subsurface is beyond the scope of this study.

For the investigation of cable effects, we want to avoid the inherent uncertainty associated to the inversion of the data. Hence, our study is based solely on the comparison of the measured phase lag (ϕ), hereafter referred to as phase for simplicity, for readings collected with different cables. We do not present plots of the apparent resistivity because all of the data collected with different cables revealed negligible differences. To present the raw data, we use a slightly modified version of the classic pseudosections, with the only difference being that the pseudosections presented here plot the actual measured phase values (ϕ) without interpolation. We believe that the pseudosections offer the best way to compare the data collected with different cables, permitting visualization of the distribution of the measurements and their spatial consistency. The expectation for "clean" data sets (e.g., without cable effects) is that the measurements should be distributed in a reduced range of values, with smooth variations along the pseudosection plane due to the (spatial) correlation between adjacent measurements (e.g., Flores Orozco et al., 2018b). Accordingly, "noisy" measurements are those in which the pseudosection shows large variability between the values in nearby measurements. We then quantify the variability in the readings by means of the standard deviation (s) of the ϕ values in the imaging data set collected for each cable and frequency after removal of erroneous measurements and outliers.

To support our expectation of smooth pseudosections independently of the complexity in subsurface architecture, we present in Figure 3 the pseudosections obtained for synthetic models with different degrees of complexity. The synthetic models are based on the expected geologic setting at the site, as resolved from wellbore data. The shape of the polarizable anomaly was modeled for the smooth and irregular geometries to investigate the resulting variations in the smoothness of the pseudosections. Our numerical investigation (see Figure 3) supports two assumptions in our study: (1) Subsurface structures with irregular shapes still result in smooth pseudosections, and (2) positive phase-lag readings (ϕ) in our measurements cannot be explained by changes in the sensitivity of the measurements and the distribution of the polarizable anomalies.

Measurements associated with a negative apparent resistivity were deleted as erroneous measurements. Similarly, positive ϕ values might be regarded as erroneous measurements, considering that those can only be explained by negative currents in a typical resistor-capacitor circuit. However, in our study, we filtered only ϕ values above 20 mrad, to take into account possible negative IP effects (for further details, refer to Dahlin and Loke, 2015; Flores Orozco et al., 2019b) and systematic patterns associated to cable effects. In addition, phase measurements below −100 mrads were also defined as outliers. This threshold value is based on a first inspection of the data collected with all the cables at P1, which revealed most of the ϕ readings in the range between −20 and 0 mrad, with a mean value of less than −7 mrads (Figure 4). Hence, the threshold value of −100 mrads was selected as a soft filter considering a potential increase in the polarization response for measurements at higher frequencies.

RESULTS

FDIP data with 5 m separation between electrodes: Comparison between long multicore and coaxial cables using a single layout and separate cables

Figure 5 shows the pseudosections after removal of outliers for data collected with the long cables along P1, i.e., for spacing of 5 m between electrodes and takeouts in the cables. Besides the pseudo-

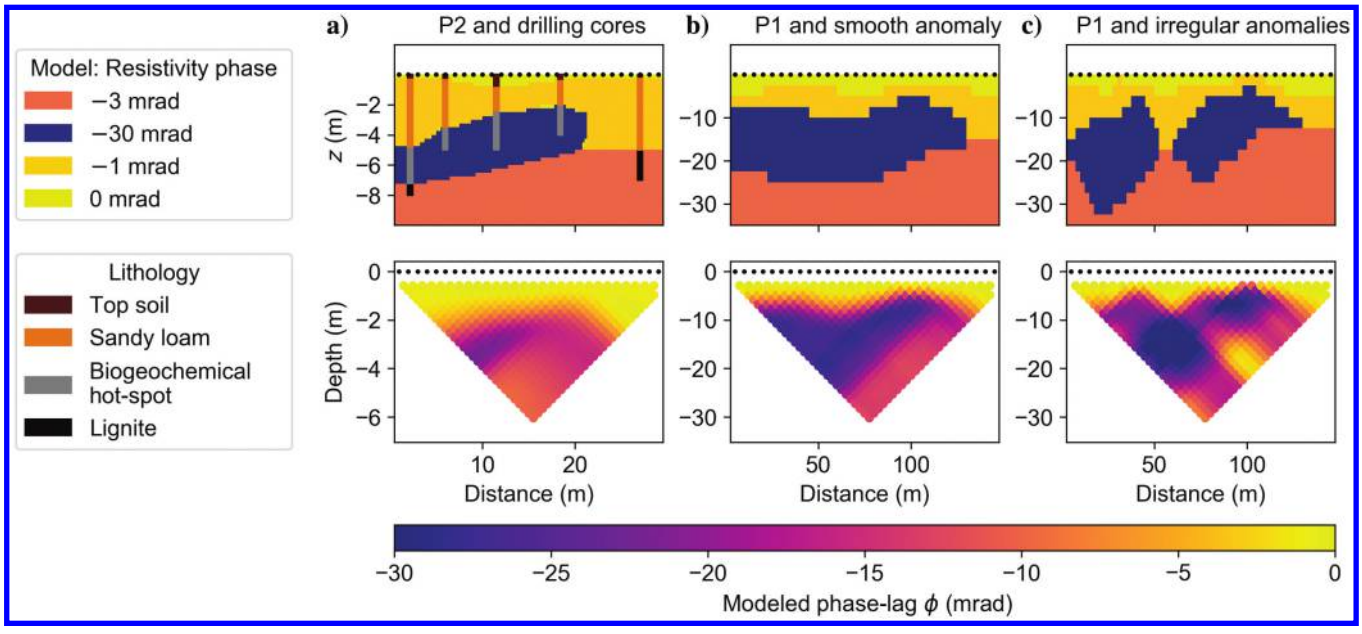

Figure 3. Numerical model to validate the assumption of smooth pseudosections. The assumed electrical units expressed in terms of the phase of the complex resistivity (top) and the pseudosections (bottom) for the modeled response, expressed in terms of the phase lag of the electrical impedance. Borehole information at the study area is imposed in the electrical model and is used to define the variations of the complex conductivity values in the subsurface.

sections obtained for measurements with different single multicore cables, we also present the pseudosections for data collected using a single coaxial cable (COAX5 and COAX10), and a separate cable layout. In the case of separate cables, we present two scenarios: (1) using two multicore cables for current (MCY5) and potential (MCZ5) readings and (2) using the combination of coaxial for current injection and multicore cables (MCY5) for potential readings. In general, Figure 5 shows smooth pseudosections for measurements collected at the lowest frequency (0.5 Hz) within the first eight levels (pseudodepth $\leq$ 10m) in which most of the phase readings are found in the range of values between −20 and 0 mrad. A similar distribution is also observed for readings collected at 1 Hz, yet the single multicore data sets reveal an increase in the variability of the readings (s increasing from approximately 18 to 22) and a larger number of spatially inconsistent measurements (i.e., noise) even within the first eight levels. The lack of spatially consistent deeper measurements (e.g., >10 m in the pseudosection) corresponds to quadrupoles associated with a poor S/N. However, measurements collected with the coaxial cables — and to some extent with separate cables — show a clean (i.e., smooth) pseudosection even for a pseudodepth of 20 m, still evidencing a good S/N. Furthermore, measurements at 1 Hz collected with a single coaxial — and to lesser extent with separate cables — still evidence a high S/N and consistent readings up to 18 levels (a maximum pseudodepth of approximately 20 m). These observations make it clear that cable effects dominate 1 Hz measurements conducted with single multicore cables and separations larger than 35 m between current and potential dipoles (corresponding to seven times the electrode spacing).

The high number of measurements removed as outliers for data collected with multicore cables (between 40% and 45%) at the low frequencies points to clear systematic errors related to the cables, considering that at such low frequencies induction effects in the shallow soils might be negligible. This is particularly evidenced by the high quality revealed by the data collected with coaxial cables (and to a certain extent with separate cables), in which less than 25% of the readings are removed as outliers, with consistent readings still visible for the larger separations between current and potential dipoles. Moreover, data collected with a coaxial cable two times larger than the actual length of the profile (10 m separation

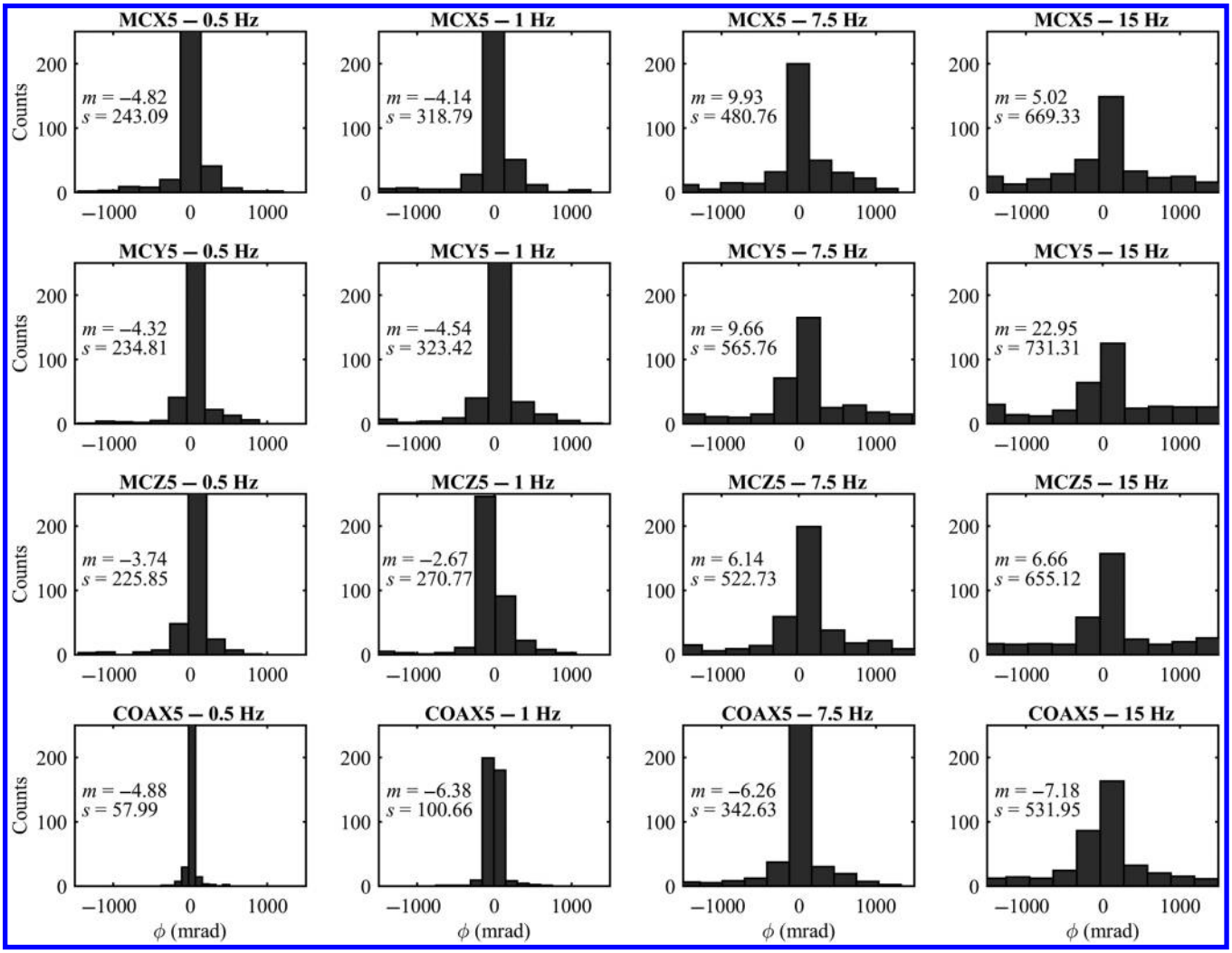

Figure 4. Histograms of the phase-lag readings in SIP measurements collected along profile P1 (5 m electrode spacing) with the long multicore and coaxial cables (5 m between takeouts). The median (m) and standard deviation (s, in mrad) for each imaging data set are indicated in each plot.

DOI:10.1190/geo2019-0552.1

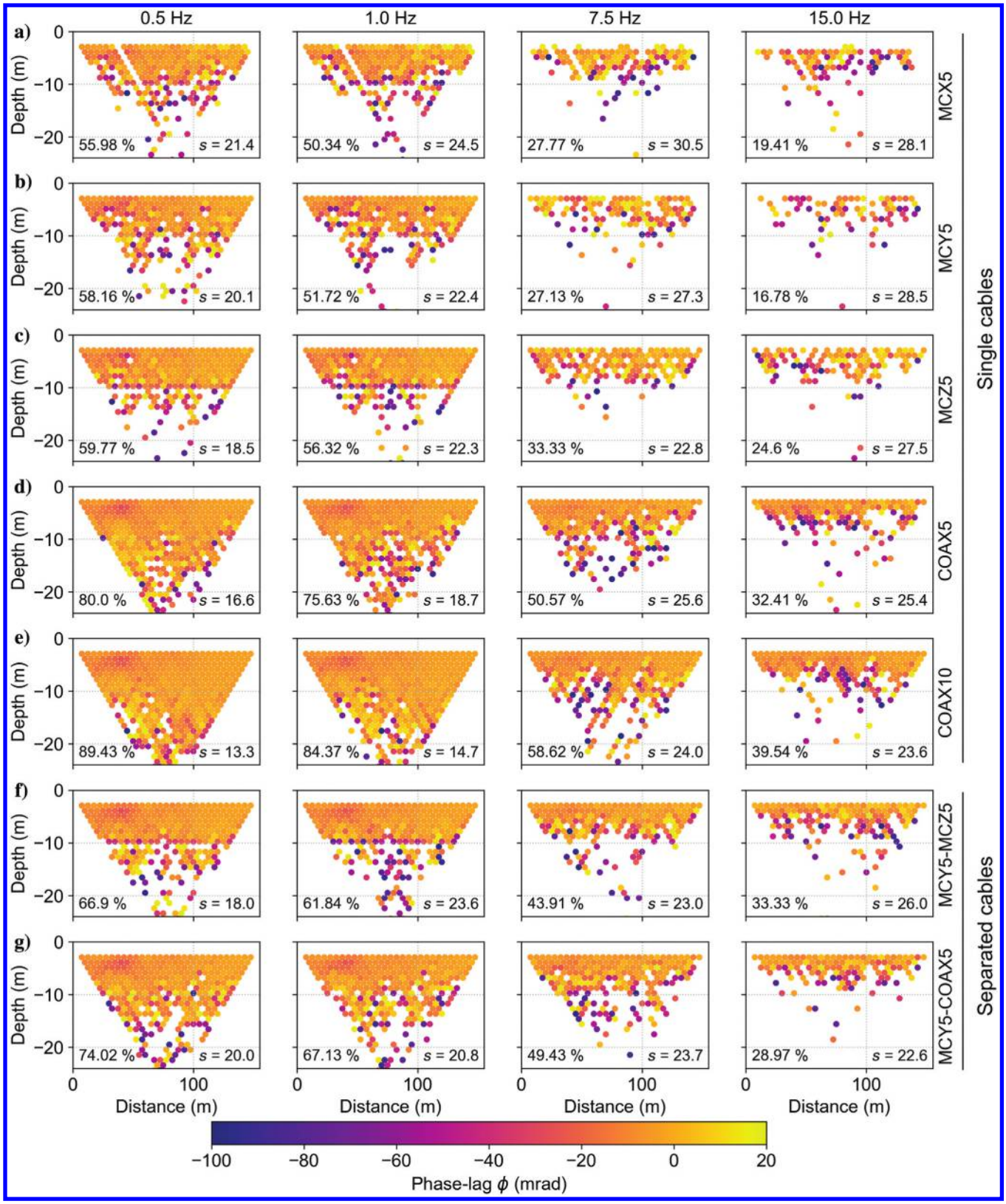

Figure 5. Pseudosections for SIP data collected at the HOAL site using 32 electrodes deployed with a separation of 5 m. SIP measurements were conducted using long multicore (MCX5, MCY5, and MCZ5) and coaxial cables (a total length of 155 m). Labels inserted show the percentage of remaining measurements after removal of outliers and the standard deviation (s) in the phase readings.

DOI:10.1190/geo2019-0552.1

between takeouts) reveal smoother pseudosections (with a lower standard deviation in the readings) and a lower number of filtered outliers than measurements collected with single multicore cables.

At 7.5 Hz, the coaxial cable still acquires data characterized by clean pseudosections for the first eight levels (e.g., a pseudodepth of 10 m), which are comparable only to the readings collected with separate cables. For measurements collected at 15 Hz, the pseudosection for the coaxial cables still shows many measurements within the first eight levels (i.e., the first 10 m of pseudodepth) with a high spatial consistency (i.e., smooth pseudosection), whereas most of the deeper measurements are removed as outliers. At 15 Hz, all multicore cables show poor performance, with more than 75% of the readings removed, and the remaining readings revealing a poor spatial consistency, with noisy pseudosections. The MCZ5 cables perform the best among the multicore cables, yet they reveal much more scattered readings and a higher number of removed outliers compared with the data set collected with the coaxial cables. Clearly, cable effects are the main reason underlying the poor quality in data collected at 1 Hz with single multicores, with a larger decrease in the quality and spatial consistency of ϕ readings at higher frequencies.

Surprisingly, SIP readings collected with two separate multicore cables reveal noisier pseudosections than those collected with a single coaxial one. This is unexpected, considering that EM coupling between wires decreases with increasing the separation between them (see equations 1 and 2) and both multicores were laid with a relatively large separation (approximately 50 cm). This observation may suggest that inductive coupling in conductive soils (such as those in the HOAL) plays a dominant role in the distortion of SIP readings collected with common multicore cables, even if different cables are used for current and potential dipoles. Accordingly, Figure 5 shows that the use of coaxial cables significantly improves the quality of SIP imaging readings over those collected with multicore cables. Measurements with separate cables can be improved using a coaxial cable. However, measurements at 7.5 and 15 Hz reveal relatively similar data quality within the first eight levels (i.e., up to 10 m depth in the pseudosection) when performed with a single coaxial cable and the combinations of the MCY5 coaxial. Nonetheless, at 0.5 and 1 Hz, only the measurements with a single coaxial cable provide clean pseudosections (including the deepest measurements).

Plots in Figure 5 reveal that SIP field surveys conducted with long multicore cables and electrode spacing (i.e., 5 m) might be limited in their depth of investigation due to the occurrence of cable effects in readings with a relatively large separation between the current and potential dipoles. Contrary to this, measurements collected with single coaxial cables are less affected by EM coupling. Moreover, the pseudosections presented in Figure 5 suggest that MCY5 cables might not be suited for collection of SIP data.

FDIP data with 1 m separation between electrodes: Comparison between long multicore and coaxial cables using single layout and separate cables

Figure 6 presents the pseudosections for measurements collected with the long cables (5 m spacing between the takeouts), but for an electrode separation of 1 m in P2. A shorter separation between electrodes favors a higher S/N and may help to reduce the contamination of the data due to EM coupling with the conductive soils. However, the long cables cannot be fully extended; thus, the exceeding cable was laid as perpendicular as possible to the profile.

As expected, the small separation between electrodes resulted in higher voltage readings, ranging between 0.5 mV and 1 V (data not shown), which are two orders of magnitude higher than those observed for measurements collected with 5 m separation between electrodes (data not shown). Given the enhanced S/N, Figure 6 reveals only minimal readings removed as outliers in the lower frequencies (0.5 and 1.0 Hz) for single multicore measurements (<30%). Moreover, pseudosections for data collected at 7.5 Hz show more than 50% valid readings for all multicore cables deployed, with the exception of MCY5. However, coaxial cables still perform the best, with less than 15% of the outliers removed at low frequencies (0.5 and 1.0 Hz). At higher frequencies, COAX5 measurements still reveal relatively clean pseudosections up to 7.5 Hz within the first 8–12 levels (pseudodepth <3 m). At such frequencies, MCX5 and MCY5 exhibit noisy measurements with almost 60% of the readings removed as outliers and a standard deviation of approximately 8 mrad larger than for COAX5 readings. Only measurements collected with MCZ5 show some consistency with the COAX5, suggesting the better performance of these multicore cables.

At 15 Hz, measurements collected with single MCX5 and MCY5 are scattered over a larger range ($s \sim 28$ mrad), yielding noisy pseudosections with a large number of removed measurements (>60%), indicating poor quality in the phase readings, whereas MCZ5 and coaxial cables show clean pseudosections within the first eight levels (depth <2 m in the pseudosection) and relatively consistent distribution within the readings ($s \sim 21$ mrad). Clearly, the long cables enhance EM coupling (within the cables and the conductive soils) at 15 Hz, even if the separation between electrodes is small. Nonetheless, measurements collected with coaxial cables at 15 Hz still show a clean pseudosection with only a few outliers removed within the first eight levels, suggesting that such effects might be reduced through the deployment of shielded cables, albeit the long cable length.

In the case of measurements collected with separate cables, one being coaxial, Figure 6 reveals that the combination MCY5-COAX5 performs better than COAX5-MCY5. Hence, the use of the coaxial cable for current injection results in data sets with a standard deviation of approximately 3 mrad smaller and approximately 3% fewer measurements removed as outliers in comparison to those when the coaxial cable is used to connect the potential electrodes. Such an observation might be explained as a higher EM coupling between the conductive soils and the shield of the coaxial cables (in the voltage dipoles) than the coupling between the conductive soils and the multicore cables. Nonetheless, Figure 6 shows that measurements with a single coaxial cable are comparable to those collected with separate cables. Moreover, Figure 6 demonstrates that measurements collected with a coaxial cable much longer than the actual separation between electrodes (five times longer in the case of our measurements) still provide comparable quality to measurements collected with separate cables.

FDIP data with 1 m separation between electrodes: Comparison between short multicore cables and long coaxial cables using a single layout and separate cables

Pseudosections presented in Figure 7 show the data quality in measurements collected with a short electrode separation and short

multicore cables (1 m for a total profile length of 31 m), in comparison with single long coaxial cables (COAX5, with 5 m spacing between takeouts), as well as separate short multicore cables. Measurements with MCY1 were not conducted. In general, Figure 7 shows that the data quality is significantly improved by reducing the length of the multicore cables to the exact size of the separation between electrodes.

In general, all measurements presented in Figure 7 show smooth pseudosections for all cables in the low frequencies (0.5 and 1.0 Hz), with fewer than 10% of measurements removed as outliers

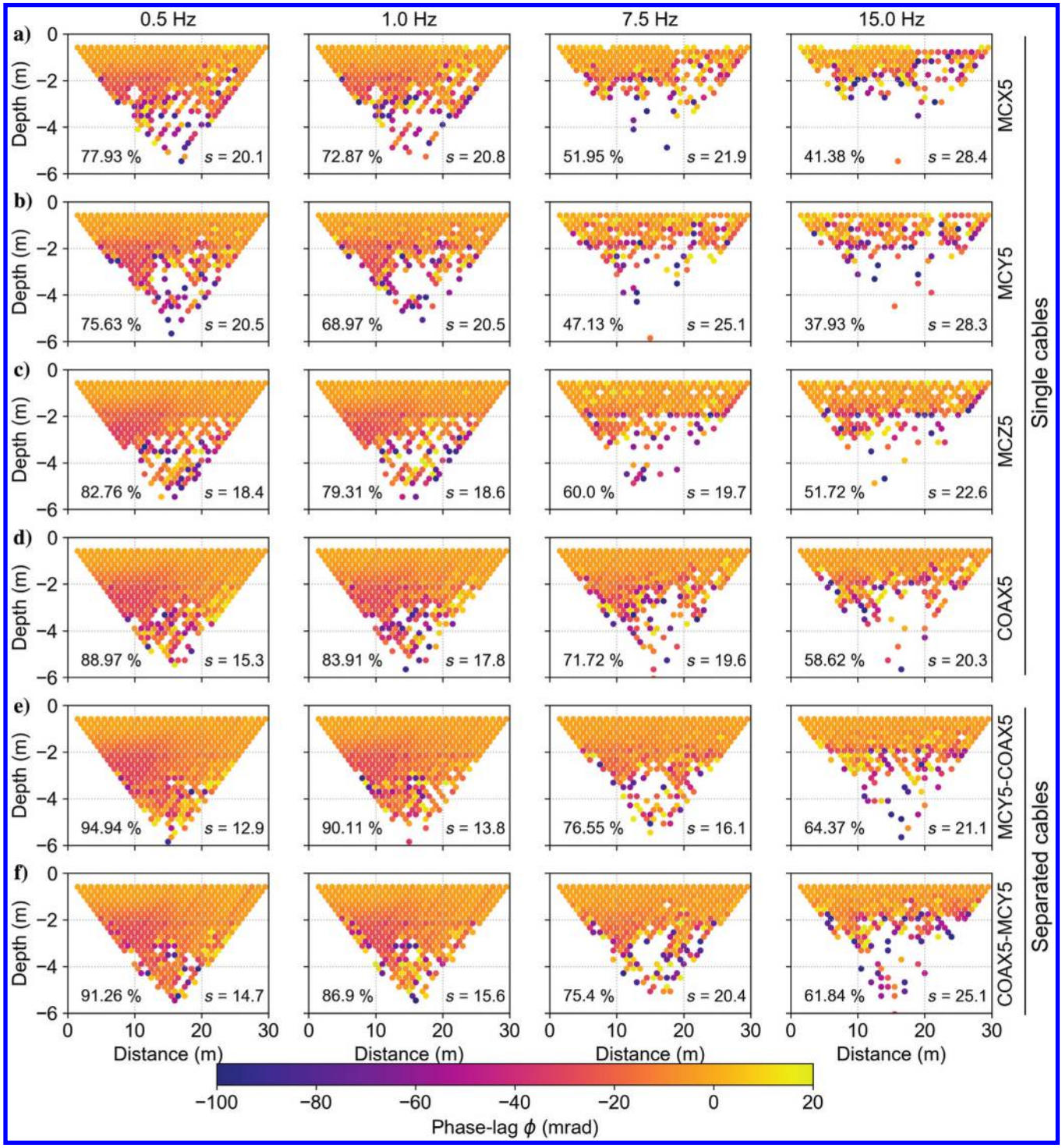

Figure 6. Pseudosections for SIP data collected at the HOAL site using 32 electrodes deployed with a separation of 1 m. SIP readings were collected using long multicore (MCX5, MCY5, and MCZ5) and coaxial cables (a total length of 115 m each). The inserted labels show the percentage of remaining measurements after removal of outliers and the standard deviation (s) in the phase readings.

for multicore cables. Moreover, pseudosections reveal consistent phase readings for 16 levels (pseudodepth <5 m) for measurements collected at low frequencies, as well as within the first 8 and 10 levels (for maximum depth of 2.5 m in the pseudosections) at high frequencies (7.5 and 15 Hz). Unavoidably, the data quality decreases with increasing the acquisition frequency for larger separations between current and potential dipoles (i.e., pseudodepth), yet in the case of short multicore cables, data collected at 15 Hz still reveal clean pseudosections only within the first eight levels (a depth of 2 m). Consistent with previous observations, the MCZ cables outperform the MCX cables.

Clearly, the short cables minimize EM coupling within the cables and possible inductive coupling with the conductive soils, permitting collection of SIP phase readings with a higher quality, even with a single multicore cable. Thus, field procedures deploying the smallest possible multicore cables are recommended to significantly improve the quality of SIP data. Contrary to this observation, data collected with a single long coaxial cable reveal still comparable pseudosections at the different frequencies, with a similar variability in the data (s varying at different frequencies between 15 and 20 mrad) and the number of removed readings as outliers. Hence, Figure 7 demonstrates that the quality of SIP measurements collected with single coaxial cables is less sensitive to the length of the cable.

Pseudosections for data collected at 0.5 and 1.0 Hz using separate short multicore cables (MCX1-MCZ1) reveal high spatial consistency between the readings ($s \sim 10$ mrad) and a minimal number of outliers (less than 5% of the readings removed). At 7.5 Hz, separate short cables still result in smooth pseudosections in almost 15 levels (i.e., a depth of 3 m in the pseudosections) and with still less than 20% of the outliers removed. In the case of data collected at 15 Hz, the use of short separate cables results in approximately 3% fewer measurements removed as outliers and a standard deviation of approximately 3 mrads smaller in comparison with the measurements with a single multicore cable. The comparison of pseudosections presented in Figures 6 and 7 shows that the deployment of multicore cables longer than the actual separation between electrodes significantly reduces the quality of SIP readings, even at low frequencies, as observed for 0.5 Hz readings with MCX5 and MCY5.

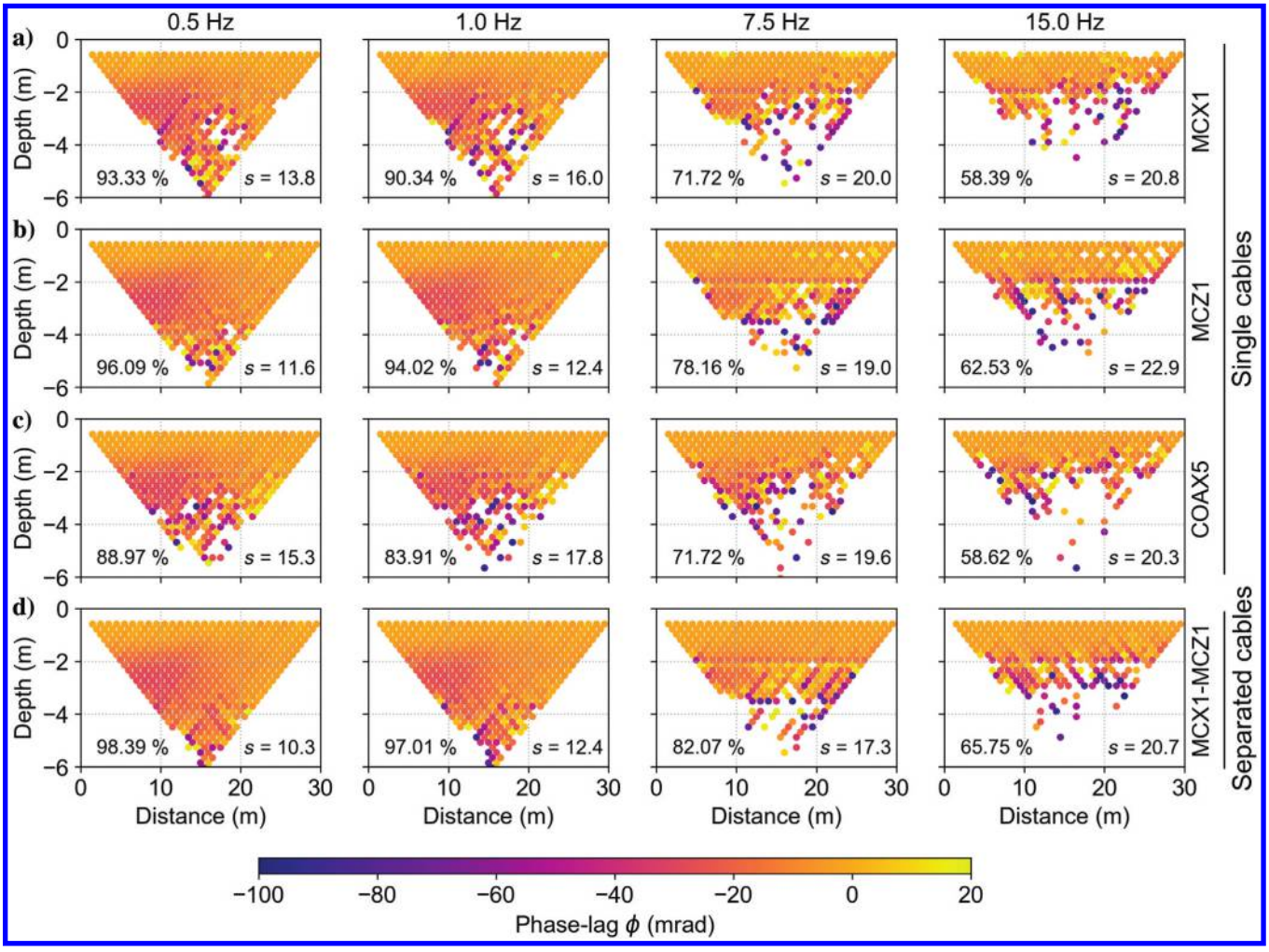

Figure 7. Pseudosections for SIP data collected at the HOAL site using 32 electrodes deployed with a separation of 1 m. SIP readings were collected using short multicore (MCX1 and MCZ1 — a total length of 31 m each) and long coaxial cables (a total length of 115 m). The inserted labels show the percentage of the remaining measurements after removal of outliers and the standard deviation (s) in the phase readings.

DOI:10.1190/geo2019-0552.1

Comparison of coaxial, multicore, and separate cables for TD measurements

Regarding EM coupling, TDIP measurements offer the advantage that potential readings are collected with a delay after the current injection is switched off, which permits minimization of EM inferences in the data. However, for completeness, here we investigate variations in the quality of the TDIP measurements collected with different cables. TDIP measurements were acquired for pulse lengths of 500 ms, using a square wave, with a 50% duty cycle. After current switch-off, the decay curve was sampled after an initial delay of 10 ms using 24 windows, with a constant width of 20 ms.

For our analysis, we present the pseudosections for chargeability measurements at three different sampling windows (2, 10, and 20 for a 500 ms pulse length), analogous to the high, intermediate, and low frequencies in FDIP. We also present pseudosections for the integral chargeability (M_{tot}), which is a quantity commonly used for the interpretation of TDIP surveys (more details can be found, for instance, in Binley and Kemna, 2005). Similar to the FDIP data, the apparent resistivity pseudosections are consistent for measurements with different cables and are not discussed here. We define and remove as outliers those measurements for which the corresponding chargeability exceeds the limits of −20 to 100 mV/V, with the broad range selected to permit the visualization of possible negative chargeability values (e.g., Dahlin and Loke, 2015) or contamination in the data due to EM coupling.

In general, Figure 8 shows clean pseudosections, at least to a depth of 4 m (at least 14 levels), and with less than 5% of the data removed as outliers (for the M_{tot} plots), clearly evidencing the good quality of the TDIP readings. As expected, the noisier pseudosections are those related to measurements collected with the long MCZ10 cables (10 m separation between takeouts for a total cable length of 310 m), which reveals the poor spatial consistency between the readings collected below 10 levels (i.e., 10 electrodes separating the current and potential electrodes). Such poor data quality might be related to cable effects or inductive coupling with the conductive soils dominating over the low voltage measurements (i.e., lower S/N). The data quality improves significantly for data collected with shorter multicore cables (from the same manufacturer), as evidenced by pseudosections for MCZ1 data. These readings show smooth pseudosections, with some noisy measurements only for the deepest measurements (below 5 m pseudodepth), TDIP measurements collected with the single coaxial cable show the smoothest pseudosections and the lowest amount of removed outliers (<1% for the M_{tot}), for all data sets collected with a single cable. However, TDIP pseudosections show in general high spatial consistency and indicate fewer outliers than the FDIP pseudosections. This is expected considering that the voltage readings are collected after the current in the transmitter is switched off, and, thus, are less affected by EM coupling, namely, by crosstalking between cables, between the transmitter and receiver in the DAS-1, and induction effects between the cables and the ground.

As expected, early IP windows (i.e., M_2 and M_{10}), reveal the largest number of filtered data (15% and 5% for long and short multicore cables, respectively, and 10% for coaxial cables), and noisy pseudosections for the readings with large levels (>4 m pseudodepth). EM coupling effects are expected in the early times (analogously to high frequencies in FDIP) and clearly affect the quality of the measurements with a weak S/N associated to a large separation between current and potential dipoles (i.e., a large pseudodepth). Such data contamination is only visible for the longest cables (MCZ10) in the integral chargeability plots, but it is almost negligible for the coaxial cable and the short multicore cable.

In Figure 8, we also present data collected with a single coaxial, two separate coaxials, two separate multicores, and separate multicore and coaxial cables, with all of these combinations revealing practically similar pseudosections (less than 3% of the data removed as outliers) with high spatial consistency ($s < 10$ mV/V) for integral chargeability values (M_{tot}). Our data show larger discrepancies in early time readings for deep measurements (pseudodepth >4 m), which are related to large separations between the current and potential dipoles, as mentioned above. EM coupling plays a more dominant role in readings at early times (i.e., M_2), analogously to the high frequencies. Accordingly, we observe a larger variation in the readings in M_2 ($s \sim 19$ mV/V) than in, e.g., M_{20} ($s \sim 13$ mV/V), as well as a larger number of measurements removed as outliers. Hence, pseudosections for M_2 provide the best overview regarding cable effects in TDIP. In such case, Figure 8 reveals that measurements collected with MCZ1 as a single cable provided the best quality, followed by readings collected with a single coaxial. Although not discussed here, further improvements in data quality could also be expected through the deploying of shorter coaxial cables, for instance, to the exact separation between electrodes.

Figure 8 also shows that coupling effects cannot be neglected in TDIP measurements, at least in early times, for instance, in the pseudosections for M_2, even if two coaxial cables are used to separate the current and potential dipoles. It might be argued that such distortions are only visible for the deep measurements, in which the lowest S/Ns are expected. However, the pseudosections (e.g., M_{20}) corresponding to later times are clean even if associated to lower chargeability values. The cable effects at early times might be relevant for the case of TDIP measurements of the full waveform, or using a 100% duty cycle, yet such discussion is beyond the scope of this study. Nonetheless, Figure 8 suggests that the use of a single short coaxial cable might also permit enhancement of the quality of the TDIP data.

DISCUSSION

Analysis of normal and reciprocal misfit

The analysis of the raw data clearly demonstrates a significant improvement in SIP readings for measurements collected with coaxial cables when compared with those acquired using multicore cables. Already for measurements at 1 Hz, imaging data sets collected with a single multicore cable result in a larger number of filtered data and a broader variance than those collected with a single coaxial cable. Moreover, it has been observed that the length of the multicore cables plays a critical role in the quality of the SIP readings, whereas this may be not relevant for measurements performed with coaxial cables. To quantitatively evaluate the data uncertainty associated to the different cables, we present in Figure 9 the analysis of misfit between normal and reciprocal phase readings ($\Delta\phi$) collected along profiles P1 and P2. Reciprocal readings refer to the recollection of a given quadrupole (i.e., normal measurements) after interchanging the electrodes used for the current and potential dipoles (LaBrecque et al., 1996). Statistical analysis of normal-reciprocal misfit ($\Delta\phi$) is a well-established method to quantify data error in electrical imaging (e.g., LaBrecque et al.,

DOI:10.1190/geo2019-0552.1

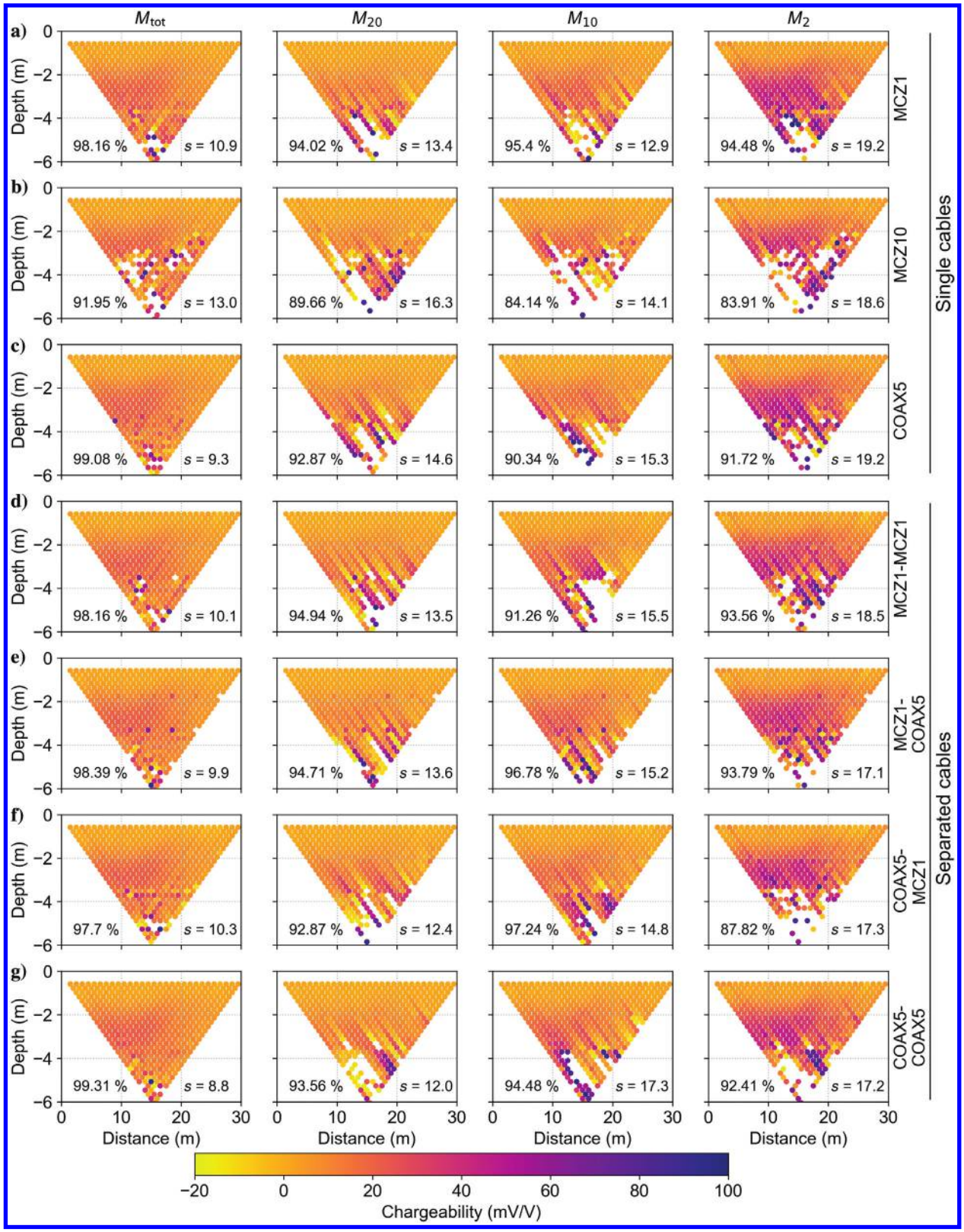

Figure 8. Pseudosections for TDIP data collected at the HOAL site using 32 electrodes with a separation of 5 m between them. TDIP readings were collected using (1) current injections and potential readings in a multicore cable (the plots in the first row) followed by (2) current injections in the multicore cable and potential readings in the coaxial (the plots in the second row). For comparison, pseudosections are also presented for data collected with a single coaxial cable (the third row). The inserted labels indicate the total of the remaining measurements after the removal of outliers and the standard deviation (s) in the phase readings.

1996; Slater and Binley, 2006; Flores Orozco et al., 2012b, 2018a, 2019b); thus, it can be used here as a tool to quantitatively compare the data collected with different cables. For the sake of consistency, in Figure 9, we compare only the $\Delta\phi$ for data collected with MCX5 and COAX10 cables along P1 (5 m spacing between electrodes), whereas MCX1 and COAX2 are compared for measurements collected along P2 (1 m separation between electrodes). In the case of multicore cables, we present measurements collected with cables having the same length as the profile (i.e., the separation between electrodes and cable takeouts being the same), whereas coaxial cables used for this analysis are always two times longer than the profile length.

During the analysis of the $\Delta\phi$, the only filtering in the data refers to the removal of erroneous measurements (readings associated with a negative apparent resistivity) and outliers (i.e., -100 mrad $< \phi <$ 20 mrad), independent of the resulting misfit between the normal and reciprocal readings. Figure 9 shows that data sets collected with coaxial cables result in a larger number of normal-reciprocal pairs (N) than measurements collected with multicore cables, along P1 and P2, and for all frequencies. At low frequencies (0.5 and 1.0 Hz), the data collected with multicore cables result in approximately 3% fewer measurements than those data sets collected with coaxial cables. Nonetheless, MCX5 and COAX10 yield similar values of the standard deviation of the reciprocal misfit ($s(\Delta\phi)$) at low frequencies (variations <1 mrad).

Measurements collected with multicore and coaxial cables at 7.5 and 15 Hz reveal consistent values in the $s(\Delta\phi)$ only for data sets collected along P2, which refers to the 1 m spacing between electrodes. However, measurements collected with the multicore cable MCX5 at P1 reveal a poor reciprocity at 7.5 and 15 Hz, with less than 30 normal-reciprocal pairs and a larger $s(\Delta\phi)$ than the data sets collected with the COAX10 cable. Moreover, such measurements exhibit a normal distribution of the $\Delta\phi$, as expected for measurements contaminated by random noise (e.g., LaBrecque et al., 1996; Slater and Binley, 2006). Such a normal distribution in the $\Delta\phi$ is also observed for all measurements collected in P2 and at low frequencies in P1. Accordingly, Figure 9 demonstrates the possibility to collect high-quality SIP imaging data with a single coaxial

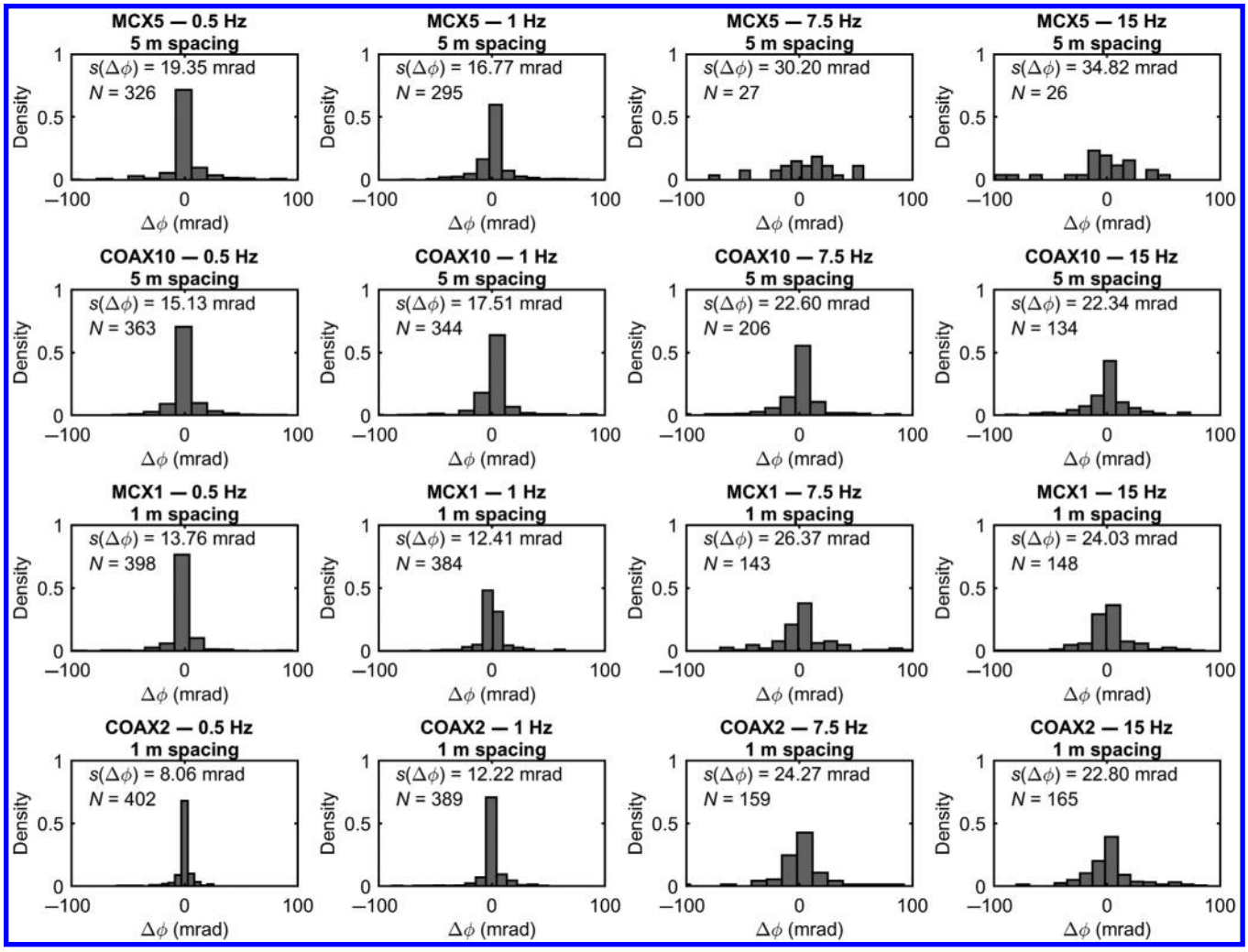

Figure 9. Analysis of the misfit between normal and reciprocal phase readings ($\Delta\Phi$) for imaging data sets collected along P1 with the long multicore MCX5 and coaxial COAX10 cables, as well as along P2 with the short multicore MCX1 and COAX2 cables. In each subplot, we include the standard deviation of the normal reciprocal misfit ($s(\Delta\phi)$) and the total number of normal-reciprocal pairs (N). Filtering of the data was performed only before the analysis of $\Delta\phi$, corresponding only to the removal of erroneous measurements and outliers.

cable, even if this is much longer than the actual length of the profile.

Comparison between coaxial and multicore cables: Implication for field surveys

Results presented in Figures 5–9 demonstrate that the use of multicore cables in SIP imaging surveys results in large distortions in the data already at 1 Hz. Moreover, measurements collected with long multicore cables reveal a poor reciprocity for readings collected at 7.5 and 15 Hz, and a larger reciprocal misfit ($\Delta\phi$) for measurements collected at 1.0 Hz in comparison to measurements collected with the coaxial cables. Distortions in the imaging data sets vary in their amplitude and distribution unsystematically for the different multicore cables deployed. Hence, removing such cable effects during the processing of the data might be impossible. Accordingly, we do not recommend the use of traditional multicore cables as a single layout for the collection of FDIP imaging data, even at 1 Hz. We believe this is an important observation, considering that 1 Hz has been suggested as the best compromise between relatively low acquisition times and negligible EM coupling.

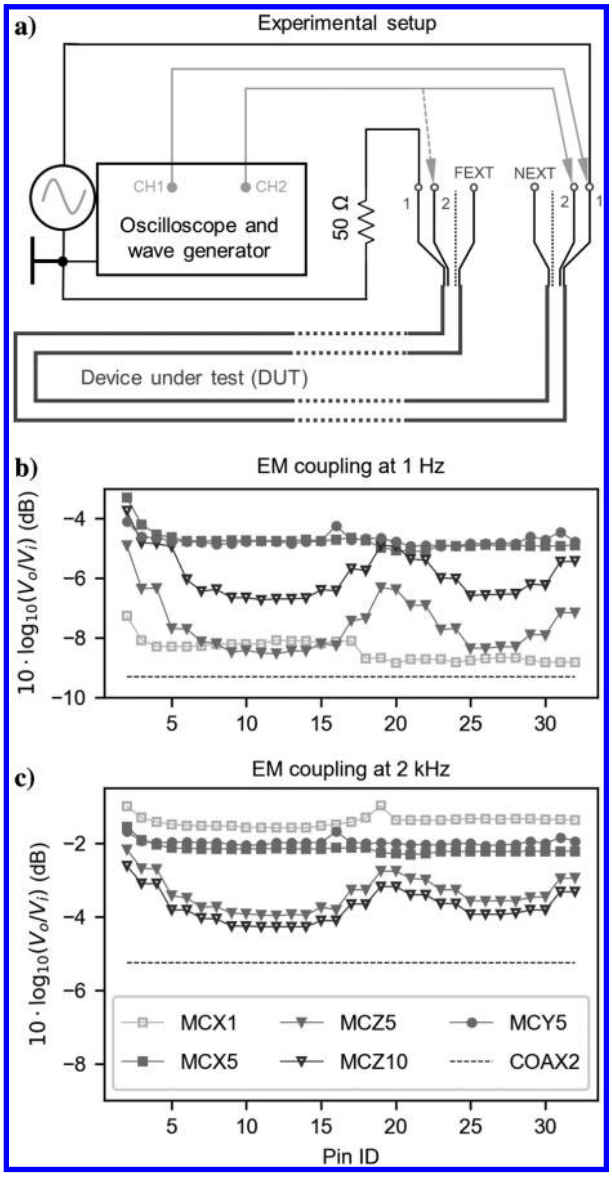

Figure 10. Pseudosections for TDIP data collected (with a pulse length of 500 ms) at the HOAL site using 32 electrodes with a separation of 1 m between them and a multicore cable with 1 and 10 m separation between takeouts (MCZ1 and MCZ10, respectively), as well as the coaxial cable with a 5 m separation between takeouts. The label indicates the total of the remaining measurements after removal of outliers and the standard deviation (s) in the phase readings.

The distortions in measurements at 1.0 Hz when using multicore cables increase with increasing the cable length, even if the cables are fully extended. We observed that the deployment of multicore cables longer than the actual separation between electrodes significantly reduces the quality of SIP readings even at low frequencies such as 0.5 Hz, independently of whether the multicore cable is used in a single layout or using two cables to separate the current and potential dipoles. Thus, the collection of reliable SIP imaging field surveys demands the use of shortest possible cables, if only multicore cables are available.

TDIP readings collected using a 50% duty cycle and multicore cables revealed the same data quality than those collected with the coaxial cables with only a minimal improvement when readings were collected with separate cables. Such measurements benefit from sampling the decay curve only after the current injection is switched off, thus minimizing the influence of parasitic EM fields. Accordingly, TDIP measurements favor the use of multicore cables. Nevertheless, chargeability measurements collected at early times revealed larger inferences (i.e., outliers) when collected with single cables than using two cables to separate the current and potential dipoles, likely indicating distortions due to coupling effects.

SIP imaging data sets collected with coaxial cables revealed an improved data quality, especially at low frequencies (0.5 and 1.0 Hz). Moreover, we observed good data quality using coaxial cables much longer than the actual profile length. Even for measurements collected with COAX10, readings revealed a significant improvement in the normal-reciprocal misfit ($\Delta\phi$) in comparison with data collected with shorter multicore cables. Moreover, measurements conducted with a single coaxial cable revealed at least the same quality as those using two multicore cables to separate the current and potential dipoles. Hence, the use of coaxial cables may represent the best alternative for field surveys, permitting use of the same cable for collection of data with different electrode spacing, as well as to double the resolution or maximum depth of investigation by avoiding the necessity to lay two different cables to separate potential and current dipoles.

The poor quality of SIP readings at frequencies greater than 15 Hz might be related to sources of contamination beyond the cable effects, such as low-frequency electrical fields associated to fluctuating telluric currents in conductive soils (Serson, 1973). Moreover, further sources of capacitive coupling can be related to variations in the contact resistances between electrodes and the soil or between electrodes and cables (Zimmermann et al., 2008, 2019). In addition, conductive soils enhance inductive coupling (e.g., Wait and Gruszka, 1986; Routh and Oldenburg, 2001).

To investigate EM coupling in multicore and coaxial cables without the interactions with subsurface materials, we performed a laboratory test. This test was conducted with each multicore cable used on the field, with the exception of the MCZ1, which is used for measurements in boreholes and the end connector is sealed. As

DOI:10.1190/geo2019-0552.1

illustrated in the schematic diagram presented in Figure 10a, we injected a sinusoidal current across one of the wires of the multicore cable with an effective input voltage (V_i) of 1 V, corresponding to a current of approximately 0.2 mA. During the current injection, we used an oscilloscope to measure the output voltage (V_o) in each one of the remaining 31 wires (against the mass of the oscilloscope). To avoid overloading the measuring channels, we connected a 50 $\pm$ 1 Ω resistance in series between the signal generator and the pins used for current injection, as illustrated in Figure 10a. For verification, readings of the V_o were collected in both end connectors, illustrated as NEXT and FEXT in Figure 10a, with the measurements in each connector corresponding to the average value of nine waveforms (commonly exhibiting fluctuations of approximately 4 mV). The experiment was repeated for all multicore cables at two different frequencies: 1 Hz and 2 kHz. Similar measurements were also conducted between the two longest wires of the COAX2 cable, yet we did not collect measurements for all wires, due to their different lengths. EM coupling in the cables is exhibited by the observed V_o in the wires of the multicore cables during the current injection, which is presented in terms of the noise at low (Figure 10b) and high (Figure 10c) frequencies.

Figure 10b and 10c shows the highest coupling for readings collected in the pin (i.e., wire) closest to the current injection, yet the distortions show erratic behavior for different wires. Nonetheless, consistent patterns can be observed for cables built by the same manufacturer, thus suggesting that such variations in the EM coupling within the multicore cables are related to the twisting of the independent wires. Similar to the field results, the shortest cable, i.e., MCX1, reveals the lowest EM coupling, whereas MCY5 exhibits the highest coupling. The longest cable tested (MCZ10) reveals intermediate coupling values, which can be explained by the high electrical resistance measured in the wires (Table 1). As expected, coupling is approximately two orders of magnitude higher for current injections at 2 kHz than at 1 Hz. Moreover, coupling in the coaxial cables is at least one order of magnitude smaller than the one observed in the MCX1. Hence, the results presented in Figure 10b support our field observations and demonstrate that multicore cables can result in EM coupling even at low frequencies, causing important distortions in SIP readings.

Besides the EM coupling between cables at 1 Hz evidenced in Figure 10b, the decrease in the data quality for our SIP field measurements might point out possible coupling effects within the measuring device (i.e., within the transmitter and receiver). Such a limitation needs to be addressed in the next generation of field-scale SIP instruments. In this regard, the Multi-Source instrument (from MPT LLC) or the V-FullWaver (from Iris Instruments) may provide an improvement in the data quality for IP field surveys because they permit remotely synchronization of the transmitter and the receiver. However, the Multi-Source instrument is still under development and the V-FullWaver does not permit collection of SIP data in the FD.

Different correction methods taking into account the geometry of the cables (e.g., Zhao et al., 2013, 2014) can still be performed to further improve the quality of the phase measurements at higher frequencies, yet their application is beyond the scope of the present study. Likewise, the collection of IP data deploying other configurations characterized by higher S/N, such as Wenner or multiple gradient, are also not addressed within this study because they do not provide new insights into the discussion.

CONCLUSION

Our results demonstrate that SIP measurements conducted in the FD with multicore cables result in significant distortions in the phase readings even at low frequencies such as 0.5 and 1.0 Hz. Consistent to previous studies, the use of separate multicore cables for current and voltage readings revealed an improved data quality in comparison to single cables. However, the data quality is still dependent on the construction and length of the multicore cables deployed, with cleaner pseudosections observed only for data collected with short cables (1 m spacing in the takeouts). Contrary to those observations, data collected with a single coaxial cable revealed high data quality, even if the cable is five times longer than the actual separation between electrodes. The improved quality in SIP imaging data sets collected with coaxial cables was demonstrated through the analysis of normal and reciprocal measurements. Our study demonstrated that the use of single multicore cables with 5 m separation between electrodes resulted in less than 10% of valid normal and reciprocal measurements at 7.5 Hz, whereas more than 50% of the measurements still show reciprocity when collected with a single coaxial cable. Accordingly, the deployment of coaxial cables removes the necessity of using separate cables, consequently increasing the depth of investigations or resolution of SIP imaging surveys. Moreover, the use of coaxial cables permits to deploy the same field procedures for the collection of SIP data as used for ERT surveys. The simplification of field procedures represents an important step forward to make the SIP imaging an attractive method for applications beyond academia.

ACKNOWLEDGMENTS

Parts of this work were funded by the Austrian Federal Ministry of Science, Research and Economy (projects "Development of Geophysical Exploration Methods for the Characterization of Mine-Tailings Towards Exploitation and Exploration" and "Geophysical Exploration of Graphite Ores"). We gratefully acknowledge Lee Slater, Stefan L. Helwig, and two anonymous reviewers for their insightful comments that helped to improve the manuscript.

DATA AND MATERIALS AVAILABILITY

Data associated with this research are available and can be obtained by contacting the corresponding author.

REFERENCES

Aal, G. Z. A., L. D. Slater, and E. A. Atekwana, 2006, Induced-polarization measurements on unconsolidated sediments from a site of active hydrocarbon biodegradation: Geophysics, **71**, no. 2, H13–H24, doi: 10.1190/1.2187760.

Atekwana, E. A., and L. D. Slater, 2009, Biogeophysics: A new frontier in Earth science research: Reviews of Geophysics, **47**, RG4004, doi: 10.1029/2009RG000285.

Binley, A., J. Keery, L. Slater, W. Barrash, and M. Cardiff, 2016, The hydrogeologic information in cross-borehole complex conductivity data from an unconsolidated conglomeratic sedimentary aquifer: Geophysics, **81**, no. 6, E409–E421, doi: 10.1190/geo2015-0608.1.

Binley, A., S. S. Hubbard, J. A. Huisman, A. Revil, D. D. Robinson, K. Singha, and L. D. Slater, 2015, The emergence of hydrogeophysics for improved understanding of subsurface processes over multiple scales: Water Resources Research, **51**, 3837–3866, doi: 10.1002/2015WR017016.

Binley, A., and A. Kemna, 2005, DC resistivity and induced polarization methods, *in* Y. Rubin and S. Hubbard, eds., Hydrogeophysics: Springer, 129–156, doi: 10.1007/1-4020-3102-5_5.

Binley, A., L. D. Slater, M. Fukes, and G. Cassiani, 2005, Relationship between spectral induced polarization and hydraulic properties of saturated and unsaturated sandstone: Water Resources Research, **41**, W12417, doi: 10.1029/2005WR004202.

Blöschl, G., A. P. Blaschke, M. Broer, C. Bucher, G. Carr, X. Chen, A. Eder, M. Exner-Kittridge, A. Farnleitner, A. Flores-Orozco, and P. Haas, 2016, The Hydrological Open Air Laboratory (HOAL) in Petzenkirchen: A hypothesis-driven observatory: Hydrology and Earth System Sciences, **20**, 227–255, doi: 10.5194/hess-20-227-2016.

Börner, F. D., J. R. Schopper, and A. Weller, 1996, Evaluation of transport and storage properties in the soil and groundwater zone from induced polarization measurements: Geophysical Prospecting, **44**, 583–601, doi: 10.1111/j.1365-2478.1996.tb00167.x.

Charnock, D., 2005, Electromagnetic interference coupling between power cables and sensitive circuits: IEEE Transactions on Power Delivery, **20**, 668–673, doi: 10.1109/TPWRD.2005.844324.

Coggon, J. H., 1984, New three-point formulas for inductive coupling removal in induced polarization: Geophysics, **49**, 307–309, doi: 10.1190/1.1441665.

Corona-Lopez, D. D. J., S. Sommer, S. A. Rolfe, F. Podd, and B. D. Grieve, 2019, Electrical impedance tomography as a tool for phenotyping plant roots: Plant Methods, **15**, 15–49, doi: 10.1186/s13007-019-0438-4.

Dahlin, T., V. Leroux, and J. Nissen, 2002, Measuring techniques in induced polarisation imaging: Journal of Applied Geophysics, **50**, 279–298, doi: 10.1016/S0926-9851(02)00148-9.

Dahlin, T., and M. H. Loke, 2015, Negative apparent chargeability in time-domain induced polarisation data: Journal of Applied Geophysics, **123**, 322–332, doi: 10.1016/j.jappgeo.2015.08.012.

Doetsch, J., T. Ingeman-Nielsen, A. V. Christiansen, G. Fiandaca, E. Auken, and B. Elberling, 2015, Direct current (DC) resistivity and induced polarization (IP) monitoring of active layer dynamics at high temporal resolution: Cold Regions Science and Technology, **119**, 16–28, doi: 10.1016/j.coldregions.2015.07.002.

Fiandaca, G., L. M. Madsen, and P. K. Maurya, 2018, Re-parametrization of the Cole-Cole model for improved spectral inversion of induced polarization data: Near Surface Geophysics, **16**, 385–399, doi: 10.3997/1873-0604.2017065.

Flores Orozco, A., M. Bücker, M. Steiner, and J. P. Malet, 2018a, Complex-conductivity imaging for the understanding of landslide architecture: Engineering Geology, **243**, 241–252, doi: 10.1016/j.enggeo.2018.07.009.

Flores Orozco, A., J. Gallistl, M. Bücker, and K. H. Williams, 2018b, Decay curve analysis for data error quantification in time-domain induced polarization imaging: Geophysics, **83**, no. 2, E75–E86, doi: 10.1190/geo2016-0714.1.

Flores Orozco, A., A. Kemna, A. Binley, and G. Cassiani, 2019b, Analysis of time-lapse data error in complex conductivity imaging to alleviate anthropogenic noise for site characterization: Geophysics, **84**, no. 2, B181–B193, doi: 10.1190/geo2017-0755.1.

Flores Orozco, A., A. Kemna, C. Oberdörster, L. Zschornack, C. Leven, P. Dietrich, and H. Weiss, 2012a, Delineation of subsurface hydrocarbon contamination at a former hydrogenation plant using spectral induced polarization imaging: Journal of Contaminant Hydrology, **136**, 131–144, doi: 10.1016/j.jconhyd.2012.06.001.

Flores Orozco, A., A. Kemna, and E. Zimmermann, 2012b, Data error quantification in spectral induced polarization imaging: Geophysics, **77**, no. 3, E227–E237, doi: 10.1190/geo2010-0194.1.

Flores Orozco, A., V. Micić, M. Bücker, J. Gallistl, T. Hofmann, and F. Nguyen, 2019a, Complex-conductivity monitoring to delineate aquifer pore clogging during nanoparticles injection: Geophysical Journal International, **218**, 1838–1852, doi: 10.1093/gji/ggz255.

Flores Orozco, A., M. Velimirovic, T. Tosco, A. Kemna, H. Sapion, N. Klaas, R. Sethi, and L. Bastiaens, 2015, Monitoring the injection of microscale zerovalent iron particles for groundwater remediation by means of complex electrical conductivity imaging: Environmental Science and Technology, **49**, 5593–5600, doi: 10.1021/acs.est.5b00208.

Flores Orozco, A., K. H. Williams, and A. Kemna, 2013, Time-lapse spectral induced polarization imaging of stimulated uranium bioremediation: Near Surface Geophysics, **11**, 531–544, doi: 10.3997/1873-0604.2013020.

Flores Orozco, A., K. H. Williams, P. Long, S. S. Hubbard, and A. Kemna, 2011, Using complex resistivity imaging to infer biogeochemical processes associated with bioremediation of an uranium-contaminated aquifer: Journal of Geophysical Research, Biogeosciences, **116**, G03001, doi: 10.1029/2010JG001591.

Gallistl, J., M. Weigand, M. Stumvoll, D. Ottowitz, T. Glade, and A. Flores Orozco, 2018, Delineation of subsurface variability in clay-rich landslides through spectral induced polarization imaging and electromagnetic methods: Engineering Geology, **245**, 292–308, doi: 10.1016/j.enggeo.2018.09.001.

Gasperikova, E., and H. F. Morrison, 2001, Mapping of induced polarization using natural fields: Geophysics, **66**, 137–147, doi: 10.1190/1.1444888.

Günther, T., and T. Martin, 2016, Spectral two-dimensional inversion of frequency-domain induced polarization data from a mining slag heap: Journal of Applied Geophysics, **135**, 436–448, doi: 10.1016/j.jappgeo.2016.01.008.

Hallof, P. G., 1974, The IP phase measurement and inductive coupling: Geophysics, **39**, 650–665, doi: 10.1190/1.1440455.

Hördt, A., R. Blaschek, A. Kemna, and N. Zisser, 2007, Hydraulic conductivity estimation from induced polarisation data at the field scale — The Krauthausen case history: Journal of Applied Geophysics, **62**, 33–46, doi: 10.1016/j.jappgeo.2006.08.001.

Huisman, J. A., E. Zimmermann, O. Esser, F. H. Haegel, A. Treichel, and H. Vereecken, 2016, Evaluation of a novel correction procedure to remove electrode impedance effects from broadband SIP measurements: Journal of Applied Geophysics, **135**, 466–473, doi: 10.1016/j.jappgeo.2015.11.008.

Kemna, A., A. Binley, C. Cassiani, E. Niederleithinger, A. Revil, L. D. Slater, W. Williams, A. Flores Orozco, F. H. Haegel, A. Hoerdt, and S. Kruschwitz, 2012, An overview of the spectral induced polarization method for near-surface applications: Near Surface Geophysics, **10**, 453–468, doi: 10.3997/1873-0604.2012027.

Kemna, A., A. Binley, A. Ramirez, and W. Daily, 2000, Complex resistivity tomography for environmental applications: Chemical Engineering Journal, **77**, 11–18, doi: 10.1016/S1385-8947(99)00135-7.

LaBrecque, D. J., M. Miletto, W. Daily, A. Ramirez, and E. Owen, 1996, The effects of noise on Occam's inversion of resistivity tomography data: Geophysics, **61**, 538–548, doi: 10.1190/1.1443980.

Martin, T., and T. Günther, 2013, Complex resistivity tomography (CRT) for fungus detection on standing oak trees: European Journal of Forest Research, **132**, 765–776, doi: 10.1007/s10342-013-0711-4.

Ntarlagiannis, D., K. H. Williams, L. D. Slater, and S. S. Hubbard, 2005, Low-frequency electrical response to microbial induced sulfide precipitation: Journal of Geophysical Research, Biogeosciences, **110**, G02009, doi: 10.1029/2005jg000024.

Olsson, P. I., G. Fiandaca, K. P. Maurya, T. Dahlin, and E. Auken, 2019, Effect of current pulse duration and recovering unbiased, quantitative induced polarization models from time-domain full-response and integral chargeability data: Geophysical Journal International, **218**, 1739–1747, doi: 10.1093/gji/ggz236.

Pelton, W. H., S. H. Ward, P. G. Hallof, W. R. Sill, and P. H. Nelson, 1978, Mineral discrimination and removal of inductive coupling with multifrequency IP: Geophysics, **43**, 588–609, doi: 10.1190/1.1440839.

Radic, T., 2016, New modular multi-channel field equipment for SIP measurements up to 20 kHz: Near Surface Geoscience 2016 — 22nd European Meeting of Environmental and Engineering Geophysics, doi: 10.3997/2214-4609.201602003.

Revil, A., and N. Florsch, 2010, Determination of permeability from spectral induced polarization in granular media: Geophysical Journal International, **181**, 1480–1498, doi : 10.1111/J.1365-246X.2010.04573.X.

Revil, A., M. Karaoulis, T. Johnson, and A. Kemna, 2012a, Some low-frequency electrical methods for subsurface characterization and monitoring in hydrogeology: Hydrogeology Journal, **20**, 617–658, doi: 10.1007/s10040-011-0819-x.

Revil, A., E. Atekwana, C. Zhang, A. Jardani, and S. Smith, 2012b, A new model for the spectral induced polarization signature of bacterial growth in porous media: Water Resources Research, **48**, W09545, doi: 10.1029/2012WR011965.

Routh, P. S., and D. W. Oldenburg, 2001, Electromagnetic coupling in frequency-domain induced polarization data: A method for removal: Geophysical Journal International, **145**, 59–76, doi: 10.1111/j.1365-246X.2001.00384.x.

Seigel, H., M. Nabighian, D. S. Parasnis, and K. Vozoff, 2007, The early history of the induced polarization method: The Leading Edge, **26**, 312–321, doi: 10.1190/1.2715054.

Serson, P. H., 1973, Instrumentation for induction studies on land: Physics of the Earth and Planetary Interiors, **7**, 313–322, doi: 10.1016/0031-9201(73)90057-5.

Slater, L., and A. Binley, 2006, Synthetic and field-based electrical imaging of a zerovalent iron barrier: Implications for monitoring long-term barrier performance: Geophysics, **71**, no. 5, B129–B137, doi: 10.1190/1.2235931.

Slater, L., A. Binley, W. Daily, and R. Johnson, 2000, Cross-hole electrical imaging of a controlled saline tracer injection: Journal of Applied Geophysics, **44**, 85–102, doi: 10.1016/S0926-9851(00)00002-1.

Slater, L., D. Ntarlagiannis, Y. R. Personna, and S. S. Hubbard, 2007, Pore-scale spectral induced polarization signatures associated with FeS biomineral transformations: Geophysical Research Letters, **34**, L21404, doi: 10.1029/2007GL031840.

Telford, W. M., L. P. Geldart, and R. E. Sheriff, 1990, Applied geophysics: Cambridge University Press 1.

Wait, J. R., and T. P. Gruszka, 1986, On electromagnetic coupling "removal" from induced polarization surveys: Geoexploration, **24**, 21–27, doi: 10.1016/0016-7142(86)90016-5.

Weigand, M., and A. Kemna, 2019, Imaging and functional characterization of crop root systems using spectroscopic electrical impedance measurements: Plant and Soil, **435**, 201–224, doi: 10.1007/s11104-018-3867-3.

Weller, A., L. Slater, S. Nordsiek, and D. Ntarlagiannis, 2010, On the estimation of specific surface per unit pore volume from induced polarization: A robust empirical relation fits multiple data sets: Geophysics, **75**, no. 4, WA105–WA112, doi: 10.1190/1.3471577.

Williams, K. H., A. Kemna, M. J. Wilkins, J. Druhan, E. Arntzen, A. L. N'Guessan, P. E. Long, S. S. Hubbard, and J. F. Banfield, 2009, Geophysical monitoring of coupled microbial and geochemical processes during stimulated subsurface bioremediation: Environmental Science and Technology, **43**, 6717–6723, doi: 10.1021/es900855j.

Williams, K. H., D. Ntarlagiannis, L. D. Slater, A. Dohnalkova, S. S. Hubbard, and J. F. Banfield, 2005, Geophysical imaging of stimulated microbial biomineralization: Environmental Science & Technology, **39**, no. 19, 7592–7600.

Zhao, Y., E. Zimmermann, J. A. Huisman, A. Treichel, B. Wolters, S. van Waasen, and A. Kemna, 2013, Broadband EIT borehole measurements with high phase accuracy using numerical corrections of electromagnetic coupling effects: Measurement Science and Technology, **24**, 085005, doi: 10.1088/0957-0233/24/8/085005.

Zhao, Y., E. Zimmermann, J. A. Huisman, A. Treichel, B. Wolters, S. van Waasen, and A. Kemna, 2014, Phase correction of electromagnetic coupling effects in cross-borehole EIT measurements: Measurement Science and Technology, **26**, 015801, doi: 10.1088/0957-0233/26/1/015801.

Zimmermann, E., J. A. Huisman, A. Mester, and S. van Waasen, 2019, Correction of phase errors due to leakage currents in wideband EIT field measurements on soil and sediments: Measurement Science and Technology, **30**, 084002, doi: 10.1088/1361-6501/ab1b09.

Zimmermann, E., A. Kemna, J. Berwix, W. Glaas, and H. Vereecken, 2008, EIT measurement system with high phase accuracy for the imaging of spectral induced polarization properties of soils and sediments: Measurement Science and Technology, **19**, 094010, doi: 10.1088/0957-0233/19/9/094010.

Biographies and photographs of the authors are not available.

DOI:10.1190/geo2019-0552.1